HHS Public Access

Author manuscript

Curr Biol. Author manuscript; available in PMC 2022 September 13.

Published in final edited form as:

Curr Biol. 2021 September 13; 31(17): 3943–3951.e3. doi:10.1016/j.cub.2021.06.040.

Sensory cilia act as a specialized venue for regulated extracellular vesicle biogenesis and signaling

Juan Wang[1], **Inna A. Nikonorova**[1], **Malan Silva**[2], **Jonathon D. Walsh**[1], **Peter E. Tilton**[1], **Amanda Gu**[1], **Jyothi S. Akella**[1], **Maureen M. Barr**[1]

[1]Department of Genetics and Human Genetics Institute of New Jersey, Rutgers University, Piscataway, NJ 08854, USA

[2]School of Biological Sciences, University of Utah, Salt Lake City, UT 84112, USA.

summary

Ciliary extracellular vesicle (EV) shedding is evolutionarily conserved. In *Chlamydomonas* and *C. elegans,* ciliary EVs act as signaling devices [1–3]. In cultured mammalian cells, ciliary EVs regulate ciliary disposal but also receptor abundance and signaling, ciliary length, and ciliary membrane dynamics [4–7]. Mammalian cilia produce EVs from the tip and along the ciliary membrane [8,9]. This study aimed to determine the functional significance of shedding at distinct locations and to explore ciliary EV biogenesis mechanisms. Using Airyscan super resolution imaging in living *C. elegans* animal model, we find that neuronal sensory cilia shed TRP polycystin-2 channel PKD-2::GFP-carrying EVs from two distinct sites - the ciliary tip and the ciliary base. Ciliary tip shedding requires distal ciliary enrichment of PKD-2 by the myristoylated coiled-coil protein CIL-7. Kinesin-3 KLP-6 and intraflagellar transport (IFT) kinesin-2 motors are also required for ciliary tip EV shedding. A big unanswered question in the EV field is how cells sort EV cargo. Here, we show that two EV cargoes – the myristoylated CIL-7 protein and PKD-2 – localized and trafficked differently along cilia and were sorted to different environmentally-released EVs. In response to mating partners, *C. elegans* males modulate EV cargo composition by increasing the ratio of PKD-2 to CIL-7 EVs. Overall, our study indicates that the cilium and its trafficking machinery act as a specialized venue for regulated EV biogenesis and signaling.

Graphical Abstract

Correspondence to Juan Wang (juwang07@hginj.rutgers.edu) and Maureen M. Barr (mmbarr@hginj.rutgers.edu). Lead contact: Maureen M. Barr (mmbarr@hginj.rutgers.edu). Twitter handle: @Barr_lab.

Author contributions

J.W., I.A.N., M.S. J.D.W, P.T, A.G., J.A. and M.B. planned and designed the research, wrote the manuscript, and helped with the data analysis. M.B. supervised all processes.

Declaration of interests

The authors declare no competing interests.

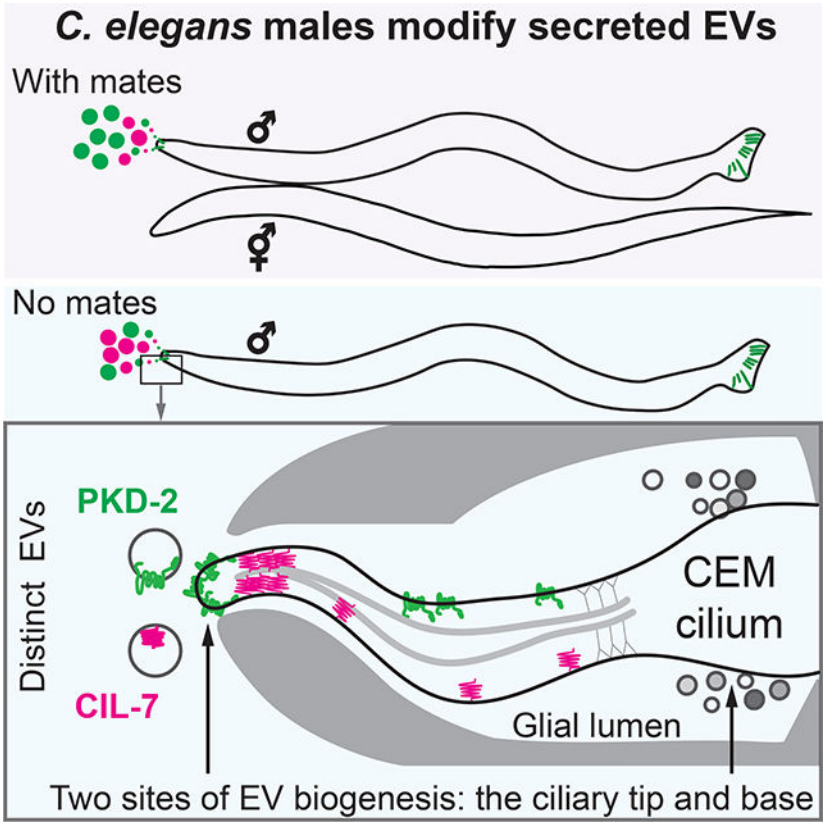

Wang *et al.* show that sensory cilia shed EVs from the ciliary tip and the periciliary membrane at the base. *C. elegans* males release distinct EVs containing signaling and biogenesis cargoes from the ciliary tip into the environment and modify the content of secreted EVs in response to the presence of mating partners.

Keywords

C. elegans ; cilia; extracellular vesicles; ectosomes; exosomes; polycystin; super resolution microscopy; kinesin-2; kinesin-3; myristoylation

Results

Autosomal dominant polycystic kidney disease gene product, polycystin-2, localizes to cilia and extracellular vesicles (EVs) throughout evolution. Loss of ciliary localization of polycystin-2 leads to cystogenesis in a mouse model [10]. The relationship between polycystin-2 ciliary localization and EV biogenesis represents a knowledge gap in the field. *C. elegans* ciliated sensory neurons release environmental EVs carrying PKD-2::GFP as visualized by live imaging. EVs are also shed at the ciliary base into the lumenal compartment formed by glial cells enwrapping neuron receptive endings as visualized by transmission electron microscopy and tomography [2,11]. The sites and mechanisms regulating ciliary EV biogenesis are not well understood.

To study ciliary EV biogenesis and shedding, we used Airyscan super-resolution microscopy to visualize fluorescently-labeled EV cargo in real time from living animals. We generated transgenic animals co-expressing PKD-2::GFP with markers that labeled the ciliary axoneme (β-tubulin TBB-4::tdTomato) or transition zone (nephrocystin-1 NPHP-1::dsRed). Analysis of PKD-2::GFP distribution relative to the markers of ciliary compartments revealed two sites of the PKD-2 EV biogenesis, the ciliary tip and ciliary base. Environmental PKD-2::GFP-carrying EVs were shed from the ciliary tip (Figure 1A, white arrowheads) and accompanied by PKD-2::GFP at the ciliary tip, along the ciliary membrane, and in periciliary membrane (PCM) at the ciliary base (Figure 1A–B, Video S1). At the ciliary base, individual EVs were captured in the process of budding from a protrusion at the PCM below the ciliary transition zone (Figure 1C–D, Video S2). All cilia shed base EVs (n=35) while 25/35 cilia shed tip EVs and 10/35 did not shed tip EVs (Table S1).

Ciliary base EVs contained both PKD-2::GFP and TBB-4::tdTomato or NPHP-1::dsRed. In contrast environmentally released EVs did not visibly carry TBB-4 or NPHP-1 (Figure 1A–B, Video S1–2), suggesting that ciliary tip and ciliary base EVs may carry different cargo and may use overlapping and different biogenesis machineries. TBB-4::tdTomato in the ciliary base EVs was continuous with PCM (Figure 1C), suggesting that the ciliary base EVs were captured in the process of budding from PCM. Budding of the ciliary base EVs from the PCM is consistent with our prior observations of EV presence in the glial lumen of the male CEM sensillum by transmission electron microscopy [2]. These data taken together suggested that cilia shed PKD-2 EVs at two sites: the ciliary tip and the PCM at the ciliary base (Figure 1E).

To explore the relationship between EVs shed from the ciliary tip and from the ciliary base, we quantified the relative distribution of PKD-2::GFP between the environmental EVs, the ciliary membrane, and the ciliary base (Table S1). Enrichment of PKD-2::GFP along the ciliary membrane positively correlated with the quantity of the environmental EVs (Figure 1F), suggesting that PKD-2::GFP must be incorporated into the ciliary membrane in order to be shed in environmental EVs. On the other hand, the relative amount of PKD-2::GFP at the ciliary base inversely correlated with the presence of PKD-2::GFP in the ciliary membrane (Figure 1G). These data suggest that environmental EV biogenesis involves a mechanism for translocating PKD-2::GFP from the PCM, along the ciliary membrane, to the ciliary tip.

To identify mechanisms driving PKD-2 protein to the ciliary tip, we focused on two gene products required for environmental release of PKD-2::GFP EVs but not for ciliogenesis: the myristoylated coiled-coil protein CIL-7 and the kinesin-3 KLP-6. In wild-type animals, PKD-2 was distributed along the length of the cilium and was enriched at the ciliary tip (Figure 2A). In the *cil-7* mutant, excessive amounts of PKD-2 accumulated on both the ciliary membrane and at the ciliary base (Figure 2B), where its quantity at the base was an order of magnitude higher than that on the ciliary membrane (Figure 2C). Excessive PKD-2 accumulation on the proximal part of the ciliary membrane of the *cil-7* mutant was accompanied by characteristic absence of PKD-2 from the tip of the cilium (Figure 2B comparing to Figure 2A). Visualization of the PKD-2 absent zone was made possible by using highly sensitive Airyscan detector capable of capturing autofluorescence of the cuticular pore, the landmark of the ciliary tip (Video S3). In total, 50% of the observed *cil-7*

mutant cilia (20 out of 42) had the PKD-2 absent zone at their distal ends, as opposed to only 6% (2 out of 31) of wild-type cilia (Figure 2F). The length of the discernible PKD-2 absent zone of the *cil-7* mutant ranged from 250 to 700 nm (Figure 2DF). These data show that delivery of PKD-2 to the ciliary membrane is not sufficient for its enrichment at the ciliary tip. Moreover, CIL-7 plays an important role in directing PKD-2 toward the distal tip and to environmental EVs.

To test whether CIL-7 functioned at the distal ciliary compartment, we imaged the CIL-7::tagRFP reporter co-expressed with PKD-2::GFP (Figure 2G). Lengthwise fluorescent profiling along the double-labeled cilium (from the very tip toward the proximal ciliary region) revealed that both PKD-2::GFP and CIL-7::tagRFP fluorescent signals peaked exclusively at the area adjacent to the ciliary tip (Figure 2G). PKD-2::GFP enrichment points were accompanied by the presence of the CIL-7::tagRFP enrichment points with the average distance of 246 nm between them (Figure 2G–I, Figure S1A–B (cilia #1 through #4)). The distance between the PKD-2 and CIL-7 enrichment points at the ciliary tip of wild-type animals roughly corresponded to the length of the PKD-2::GFP absent zone in the *cil-7* mutant (Figure 2D–F). These data suggested that CIL-7 acted at the distal region of the cilium, facilitating enrichment of PKD-2::GFP at the ciliary tip for its exit as environmental EVs.

How does CIL-7 presence at the distal cilium influence enrichment of PKD-2 at the ciliary tip? CIL-7 is a cargo of environmental EVs [2,12] and may be involved in the recruitment of PKD-2 into EVs containing CIL-7. To test this, we determined whether CIL-7 and PKD-2 were co-sorted into EVs and found PKD-2 and CIL-7 mostly on separate EVs (Figure S2A–B). Super-resolution imaging revealed three scenarios of PKD-2 and CIL-7 EV shedding: (i) CIL-7 EV budding from the ciliary tip without accompanying PKD-2 (Figure S2B), (ii) PKD-2 EV budding from the CIL-7 enriched area of the ciliary tip (as depicted on Figure 2G, Figure S1), and (iii) several PKD-2 EVs budding simultaneously from a large CIL-7 protrusion at the ciliary tip and separation into PKD-2 and CIL-7 carrying EVs (Figure S3). Formation of the PKD-2 EVs at the ciliary tip was always accompanied by CIL-7 distal ciliary enrichment, whereas budding of CIL-7 EVs was independent of PKD-2 presence. Combined, these data suggest that CIL-7 acts an essential component of EV launching pad by enriching PKD-2 at the ciliary tip and releasing PKD-2 into environmental EVs.

Since PKD-2- and CIL-7-carrying EVs are simultaneously released by same cilium, we asked if PKD-2 was required for CIL-7 environmental EV release. To examine native CIL-7 localization, we performed CRISPR/Cas9-mediated genome editing to fuse the endogenous *cil-7* locus to the mNeonGreen coding region. In wild type, we observed CIL-7 ciliary localization and environmental EV shedding from male-specific and sex-shared IL2 cilia (Figure 2J). CIL-7 ciliary localization and EV biogenesis were indistinguishable in *pkd-2* mutant and wild-type animals (Figure 2K, Figure S4). The results indicate that PKD-2 is not required for CIL-7-EV biogenesis in contrast for the essential role of CIL-7 in PKD-2 EV biogenesis. Components of the EV biogenesis machinery – such as Alix and Tsg101 [13] and CD9 [14] – are commonly used for EV isolation and identification, indicating that some part of the EV biogenesis machinery remains EV-associated. Likewise, CIL-7 is required for

PKD-2 EV biogenesis, yet CIL-7 and PKD-2 are found on different EVs. We propose the terms “biogenesis” and “signaling” EVs, marked by CIL-7 and PKD-2, respectively.

The continuous loss of CIL-7 from the ciliary tip during PKD-2 EV shedding suggests that distal ciliary pool of the CIL-7 protein must be maintained. Thus, we next sought to identify the mechanisms regulating PKD-2 and CIL-7 distribution in cilia. The cell-specific ciliary kinesin-3 KLP-6 is important for PKD-2 localization in cilia and in EVs but not for ciliogenesis [2,15,16]. We compared ciliary localization of PKD-2 and CIL-7 in wild type and *klp-6* mutants at the onset of PKD-2::GFP and CIL-7::tagRFP expression in the fourth larval stage (L4) of male development. The CEM neurons express genes required for ciliary axoneme specialization and sensory function at the L4 stage upon sexual maturation [11,17–20]. To avoid protein accumulation as secondary consequence of aging, we examined PKD-2 and CIL-7 localization at L4 stage to directly detect ciliary localization or EV shedding defects. In wild-type L4 cilia, PKD-2 and CIL-7 reached the ciliary tip and were shed as EVs into the environment (Figure 3A). In *klp-6* mutants, both PKD-2 and CIL-7 entered cilia but failed to locate distally and were not shed in environmental EVs (Figure 3B, D, E). In *klp-6* mutant cilia, PKD-2 formed small protrusions along areas enriched with CIL-7 (Figure 3B), supporting the hypothesis that enrichment of the CIL-7 protein drives PKD-2 EV biogenesis. The absence of strict colocalization between PKD-2 and CIL-7 suggested distinct mechanisms for ciliary localization.

To determine how PKD-2 and CIL-7 enter cilia, we imaged their fluorescent reporters in the mutants with disruption in the intraflagellar transport (IFT) motors, homodimeric kinesin-2 OSM-3 (KIF17 in mammals) and a subunit of heterotrimeric kinesin-2 KLP-11 (Figure 3C). These motors are redundantly required for PKD-2 environmental EV release [2], and therefore examination of PKD-2 and CIL-7 distribution pattern in the double mutant might inform on mechanistic aspects of PKD-2 and CIL-7 EV biogenesis. In the *osm-3 klp-11* mutant, CIL-7 but not PKD-2 entered the cilium (Figure 3C–D), suggesting that PKD-2 ciliary entry was IFT-dependent whereas CIL-7 ciliary entry was not. *osm-3 klp-11* mutants displayed substantial CIL-7::tagRFP accumulation at ciliary bases that correlated with PKD-2::GFP membrane protrusions. This phenotype resembled the PKD-2::GFP protrusions in CIL-7-enriched areas in *klp-6* mutant cilia (Figure 3B). The *osm-3 klp-11* mutant did not produce environmental PKD-2 and CIL-7 EVs (Figure 3E). Thus, PKD-2 EV biogenesis at the ciliary tip required functional IFT kinesin-2 motors to enter cilia. Once in the cilium, PKD-2 employed CIL-7- and KLP-6-dependent mechanisms to gain enrichment at the ciliary tip and to be shed into environmental EVs.

Since CIL-7 and PKD-2 are transported differently and sorted to distinct EVs, we considered the physiological significance a single ciliated cell producing heterogeneous EVs. A known stimulant for male-specific sensory neurons is presence of mating partners [21–24]. PKD-2-carrying EVs are directly transferred from males to hermaphrodites during mating [25], suggesting that PKD-2 signaling is associated with the presence of mating partners. Thus, we tested whether mating partners influenced environmental EV cargo content and release. We scored numbers of environmental EVs released by one day old virgin adult and by males from a mixed male-hermaphrodite population (Figure 4A). We observed a significant increase in the ratio of PKD-2 EV to CIL-7 EV shedding in males that were exposed to

mating partners (Figure 4B–C). The increased ratio of PKD-2 to CIL-7 EVs is not simply due to an increase in the number of EVs released by the CEMs when males are exposed to hermaphrodite mating partners. The number of CIL-7 EVs released by males exposed to mating partners decreased when compared to virgin males (Figure 4C). Our results indicate that *C. elegans* males modulate EV cargo composition in response to presence of hermaphrodite mating partners.

Discussion

Polycystin-1 and polycystin-2 localize to cilia and EVs throughout evolution [26–28]. The relationship and function of the polycystins in cilia and EVs are fundamental questions in the polycystic kidney disease field. Ciliary localization is a requirement for polycystin function in cilia, polycystin release in EVs, and for polycystin-based EV signaling (this work and [2]) Consistent with these observations, ciliary localization of polycystin-2 is essential for preventing cystogenesis in a mouse model [10]. Intriguingly, loss of cilia prevents cystogenesis in a Pkd2 mutant mouse via an unknown mechanism [29]. Our studies in “the worm” indicate that the polycystins have cell autonomous (in cilia) and non-cell autonomous (in EVs) functions, and suggest that abnormal polycystin function in cilia or EVs may contribute to pathogenesis.

The antagonistic relationship between PKD-2 EV shedding from the ciliary tip versus the base is consistent with our previous work showing that genetic disruption of environmental EV release correlates with massive ciliary base accumulation [11,12,19,30]. EV release from the ciliary tip, but not from the base, requires IFT. Thus, ciliary trafficking may regulate levels of PKD-2 EV shedding from the ciliary base and the ciliary tip. The periciliary membrane is specialized region that regulates trafficking in and out of the cilium [31,32]. In *Chlamydomonas*, the ESCRT machinery localizes to flagellar transition zones and ectosomes [33,34]. We propose that ciliary tip and base EVs may carry different cargoes and use overlapping and different biogenesis machineries. We previously showed that excessive ciliary base EV accumulation negatively impacts cephalic sensory organ and glial health [35]. Amphid glia engulf shed sensory endings of the ciliated AFD neuron and glia influence neuron shape and function [36]. Hence environmental tip EVs and internal ciliary base EVs may distinct functions in inter-organismal signaling [2,25,30,37] and neuron-glia communication, respectively.

C. elegans EV releasing cilia are specialized structurally and functionally. Cilia of EV-releasing neurons (EVNs) protrude to the environment from cuticular pores [38–40] and shed EVs in response to mechanical pressure [25]. EVN ciliary membrane homeostasis of PKD-2 is modulated by a phosphoinositide 5-phosphatase [41,42] and caveolin [43]. The tubulin code is required for the unique EVN ciliary ultrastructure and EV environmental release [11,19,42], while kinesin-3 KLP-6 regulates IFT and EV biogenesis at both the cilia base and tip [15,16]. The kinesin-3 motor family is characterized by their N-terminal motor domain, a forkhead-associated domain, and a tail possessing lipid-binding domains [44]. The KLP-6 mammalian homolog KIF13B - via its lipid-binding C2 domain - maintains a caveolin-enriched membrane domain at the ciliary base [45]. The KLP-6 tail contains positively charged amino acids [15] that may enhance protein binding to negatively charged

phospholipids in the ciliary membrane or polyglutamylated tubulin in ciliary axoneme [19,42]. We envision a mechanism whereby KLP-6 connects to the ciliary membrane and axoneme and directs myristoylated CIL-7 to the ciliary tip for EV biogenesis. Coiled-coil proteins similar to CIL-7 mediate membrane fission by inserting the amphipathic helix into a membrane bilayer [46].

C. elegans ciliary tip EV shedding displays some differences from ciliary ectocytosis [4]and ciliary tip decapitation in mammalian cell culture [5]. PKD-2-carrying EVs are released from the ciliary tip upon coverslip placement and range in number from several to hundreds (Figure S2A–B). By contrast, ciliary ectocytosis or decapitation events occur one at a time and over the course of several minutes. In IMCD3 cell culture, the KLP-6 homolog KIF13B is not required for ciliary ectocytosis of the neuropeptide Y receptor NPY2R [4]. The *Chlamydomonas* genome lacks kinesin-3 motors [47], suggesting that multiple motors regulate ciliary tip shedding.

Environmentally-released EVs are instrumental effectors used by parasitic worms to manipulate the host immune system to initiate and maintain infections [48]. The anthelmintic drug ivermectin inhibits EV secretion [49] and is considered an essential drug by the World Health Organization, yet its therapeutic mechanism of action is not clear. One current hypothesis is that ivermectin regulates the release of excretory-secretory products from parasites. In *C. elegans*, cilia-defective mutants are resistant to ivermectin [50] and do not produce PKD-2::GFP-carrying environmental EVs [2]. Here we show that *C. elegans* males modulate environmental EV cargo content and production in response to environmental cues (Figure 4), indicating that nematodes dynamically regulate environmental EVs under different physiological condition. We propose that nematodes use EV-producing ciliated sensory neurons to produce and package distinct EV cargo for signaling between animals (for example, host immunomodulation by parasites and male-hermaphrodite communication in *C. elegans*) and that ciliary regulation of EV composition and shedding may be a conserved phenomenon in the animal kingdom.

STAR★METHODS

Resource Availability

Lead contact—Further information and requests for resources and reagents should be directed to and will be fulfilled by the lead contact, Maureen Barr (barr@hginj.rutgers.edu)

Materials availability—Plasmids and transgenic *C. elegan* strains are available upon request.

Data and code availability—Microscopy data reported in this paper will be shared by the lead contact upon request.

All original code has been deposited at Zenodo and is publicly available as of the date of publication. DOI is listed in the key resources table.

Any additional information required to reanalyze the data reported in this work is available from the Lead Contact upon request.

Experimental model and subject details—*C. elegans* culture and genetics were performed as described [53]. *C. elegans* strains were maintained at 22°C on nematode growth medium (NGM) plates seeded with *Escherichia coli* (OP50 strain) as a food source.

Method details

PKD-2 and CIL-7 as EV markers—PKD-2 and CIL-7 reporters are excellent readouts of the endogenous proteins. The PKD-2::GFP transgenic reporter in this work is an integrated transgenic line that rescues *pkd-2* mutant phenotypes and is indistinguishable from anti-PKD-2 antibody staining [52,54].These transgenic lines have been established for studying PKD-2 trafficking and EV biogenesis [2,11,12,18,19,25]. CIL-7::tagRFP transgene was constructed by Gibson Cloning with forward primer 5'-ATG GAT ACG CTA ACA ACT TGG GCT GGG AGT CGA TAC ATG GT-3' and reverse primer 5'-CAG CTC TTC GCC CTT AGA CAC ATG ATG TGC AGA CTT CTT CTT TC-3' used to amplify it from genomic DNA of the natural isolate N2 as a template. Amplified fragments were cloned to the pPD95.75 vector backbone (gift from Andrew Fire, Addgene plasmid #1494) modified to carry tagRFP. Generation of extra-chromosomal array transgenes was carried out using standard procedures. The procedure included injection of a plasmid cocktail into the *pha1(e2123ts)III; him-5 V* strain. The plasmid cocktail contained the transgene-of-interest at 10 ng/μL and a rescue transgene for the temperature-sensitive mutation in the *pha-1* gene (pBX1 *pha-1+*) at 100 ng/μL. Stable line *myEx888[CIL-7::tagRFP+pBX1]* was further crossed to the *klp-6(my8)III* mutant to generate the PT3383 strain, and to the *osm-3(p802) klp-11(tm324)IV* double mutant to generate the PT3380 strain. In this work we also generated a CRISPR reporter of CIL-7. Similar to transgenic CIL-7 reporters, the CIL-7:mNeonGreen reporter displays base and tip EVs in both wild type and the *pkd-2* mutant. These results indicate that base EV biogenesis is a naturally occurring phenomenon. Moreover, our previous electron tomography analysis of wild-type CEM cilia has shown that base EV shedding occurs in wild type [2].

***cil-7::mNG* CRISPR—**To generate the *cil-7::mNeonGreen* endogenous CRISPR tags, we followed the Mello Lab protocol and used partially single-stranded dsDNA donors [55] with 35-bp of flanking homology [56] that included a short flexible linker sequence between the 3' end of *cil-7* and the start of mNeonGreen. The guide sequence was designed using CRISPOR [57, http://crispor.tefor.net/]. Reagents used are as follows. dg357 was a gift from Dominique A. Glauser and was used in accordance with the *C. elegans* group license with Allele Biotech.

Airyscan super-resolution microscopy—Super-resolution imaging was performed on the Zeiss LSM880 confocal system equipped with Airyscan Super-Resolution Detector with Fast Module, 7 Single Photon Lasers (405, 458.488, 514, 561, 594, 633nm), Axio Observer 7 Motorized Inverted Microscope, Motorized X-Y Stage with Z-Piezo, T-PMT. Planes of captured Z-stacks were distanced at 0.09 to 0.185 μm for optimal 3D rendering. Image analysis and processing was performed using Zen Blue 2.0 and Zen Black 2.0. The Imaris

9.5 (Bitplane, US) package was used to generate the three-dimensional reconstructions and surface rendering from the Airyscan processed images.

Mounting males for super resolution live animal imaging—Males were anesthetized with 10 mM levamisole solution in the M9 buffer. To completely immobilize the male, we used thin agarose pads, prepared from 10% melted agarose (Sigma #A9539) and Millipore water. Melting of 10% agarose was achieved by pulse heating in a microwave in 3 second intervals for a total of 1 minute or until dry agarose pieces were no longer visible. Once melted, the 10% agarose was incubated at 95ºC for about 10 minutes to allow air bubbles to escape. The melted agarose was dispensed onto glass slides in 100 μL droplets and the droplets were immediately pressed with a second glass slide to make a thin gel pad. The agarose pads were made in batches and stored in a sealed glass slide container at room temperature for up to a week. Prior to use, one glass slide was removed, the agarose pad was dried at room temperature until excess water was no longer visible, yet the pad remained moist. Once achieved, the agarose pad was cut into 1 cm × 1 cm square to remove dried edges and ensure even surface. Males were placed in 1 μL droplet of 10 mM Levamisole dispensed on a 18 × 18 cm coverslip, then the coverslip with males was flipped on the center of the agarose pad. Semi-dry agarose pads held the males tightly under the coverslip by capillary action and minimized worm moving.

Late L4 and young adult male preparation for super-resolution imaging the CEM cilia—About 100 – 200 L4 males were picked from a healthy *C. elegans* culture to a new seeded plate prior to imaging. Three hours later young adult males with completely developed tail fan and rays were selected for imaging. Late L4 males were picked just prior to molting when cuticle was covering the almost fully mature tail. Young adult males were defined by the absence of the molt cuticle covering their tails.

Quantification of PKD-2::GFP distribution in environmentally released EVs, ciliary shaft and ciliary base—Z-stacks of each male head to encompass CEM neuron environmental EVs, cilia and ciliary base were taken with Plan-Apochromat 63x/1.40 Oil objective with 6x Zoom acquisition area under Airyscan super resolution mode. Raw image files were processed with Airyscan Processing program in Zen Blue 2.0 or Zen Black 2.0 software. Maximum projection images of each Z-stack were analyzed by the Image Analysis Wizard program in Zen Blue software. Total fluorescence intensity of environmentally released EVs, ciliary shaft and ciliary base were recorded in excel file for data analysis.

PKD-2 absent zone quantification in the distal cilia—The distal ciliary PKD-2 absent zone in the *cil-7* mutant was determined by lengthwise fluorescence profiling analysis along the cilium from the ciliary tip to the ciliary base. In wild type, PKD-2 was enriched at the ciliary tip, the PKD-2 fluorescent signal at ciliary tip was higher than that of the ciliary membrane. In the *cil-7* mutant, the PKD-2 signal at the ciliary tip was very faint and lower than that of the ciliary membrane. PKD-2 absence in the distal cilia was defined by the distance between the fluorescence signal peak of the very faint ciliary tip to where the PKD-2 signal rises abruptly to the same level of PKD-2 signal at the ciliary tip. If the ciliary tip PKD-2 signal was higher than that of the ciliary membrane, the cilium was defined to

have no PKD-2 absent zone. Two out of 31 cilia in wild type had PKD-2 exclusion zone in the distal cilia. 20 out of 42 cilia in the *cil-7* mutant had PKD-2 absent zone, with a range of 250 to 700 nm.

PKD-2 and CIL-7 EV number and ratio quantification—Populations were synchronized by picking 10 L4 hermaphrodites on new seeded NGM plates. Three days later 20 to 30 L4 males were isolated from the mixed population to deprive males of exposure to their mating partners during the final steps of their sexual maturation. The isolated virgin males were imaged the next day (24 hours later) to quantify their capacity to release EVs. This imaging was done in parallel with imaging of adult males that were exposed to hermaphrodites until imaging time. Imaging was performed in 1 mM Levamisole prepared with ddH_2O on 5% agarose pads. Colocalization of PKD-2 and CIL-7 was defined by a distance between centroids of the fluorescent areas being less than 200 nm using a custom python script. The script is available upon request.

Quantification and statistical analysis

The Prism software package (GraphPad Software 8) was used to carry out statistical analyses. Information about statistical tests, p values and n numbers are provided in the respective figures and figure legends. When applicable normality of the data was examined using the Shapiro–Wilk normality test. All pairwise comparisons were followed with Dunn's multiple comparison for multiple testing. Significance was determined when the P-value < 0.05.

Supplementary Material

Refer to Web version on PubMed Central for supplementary material.

Acknowledgments

This work was supported by National Institutes of Health (NIH) DK059418 and DK116606 to M.M.B, a grant from Kansas PKD Research and Translation Core Center P30 DK106912 to J.W., and NIH Institutional Research and Academic Career Development Award (IRACDA) 5K12GM093854 to J.D.W. We thank Noriko Kane-Goldsmith and Tanay Desai for training and assistance with confocal microscopy; Gloria Androwski and Helen Ushakov for excellent technical assistance; Erik Jorgensen for mentoring and generosity, Barr lab mates and the Rutgers *C. elegans* community for feedback and constructive criticism throughout this project; Joel Rosenbaum and the three anonymous reviewers for insightful suggestions on this manuscript. We also thank the Wormbase and Caenorhabditis Genetics Center (CGC) for resources information and strains. The CGC is supported by the National Institutes of Health - Office of Research Infrastructure Programs (P40OD010440).

References

1. Wood CR, Huang K, Diener DR, and Rosenbaum JL (2013). The cilium secretes bioactive ectosomes. Current Biology 10, 906–911.
2. Wang J, Silva M, Haas LA, Morsci NS, Nguyen KCQ, Hall DH, and Barr MM (2014). *C. elegans* ciliated sensory neurons release extracellular vesicles that function in animal communication. Current Biology 5, 519–525.
3. Luxmi R, Kumar D, Mains RE, King SM, and Eipper BA (2019). Cilia-based peptidergic signaling. PLoS Biology 12, e3000566.
4. Nager AR, Goldstein JS, Herranz-Pé Rez V, Portran D, Ye F, Manuel Garcia-Verdugo J, Herranz-Pé V, Garcia-Verdugo J, and Nachury MV (2017). An Actin Network Dispatches Ciliary GPCRs into Extracellular Vesicles to Modulate Signaling. Cell 252–255.e14. [PubMed: 28017328]

5. Phua SC, Chiba S, Suzuki M, Su E, Roberson EC, Pusapati GV, Setou M, Rohatgi R, Reiter JF, Ikegami Ket al. (2017). Dynamic Remodeling of Membrane Composition Drives Cell Cycle through Primary Cilia Excision. Cell 1–2, 264–279.e15.
6. Salinas RY, Pearring JN, Ding JD, Spencer WJ, Hao Y, and Arshavsky VY (2017). Photoreceptor discs form through peripherindependent suppression of ciliary ectosome release. J. Cell Biol. 5, 1489–1499.
7. Molday RS, and Goldberg AFX (2017). Peripherin diverts ciliary ectosome release to photoreceptor disc morphogenesis. J. Cell Biol. 5, 1227–1229.
8. Spencer WJ, Lewis TR, Pearring JN, and Arshavsky VY (2020). Photoreceptor Discs: Built Like Ectosomes. Trends Cell Biol. 11, 904–915.
9. Kiesel P, Alvarez Viar G, Tsoy N, Maraspini R, Gorilak P, Varga V, Honigmann A, and Pigino G (2020). The molecular structure of mammalian primary cilia revealed by cryo-electron tomography. Nature Structural and Molecular Biology 27, 1115–1124.
10. Walker RV, Keynton JL, Grimes DT, Sreekumar V, Williams DJ, Esapa C, Wu D, Knight MM, and Norris DP (2019). Ciliary exclusion of Polycystin-2 promotes kidney cystogenesis in an autosomal dominant polycystic kidney disease model. Nature Communications 10, 4072.
11. Silva M, Morsci N, Nguyen KCQ, Rizvi A, Rongo C, Hall DH, and Barr MM (2017). Cell-Specific α-Tubulin Isotype Regulates Ciliary Microtubule Ultrastructure, Intraflagellar Transport, and Extracellular Vesicle Biology. Current Biology 7, 968–980.
12. Maguire JE, Silva M, Nguyen KCQ, Hellen E, Kern AD, Hall DH, and Barr MM (2015). Myristoylated CIL-7 regulates ciliary extracellular vesicle biogenesis. Mol. Biol. Cell 15, 2823–2832.
13. Van Niel G, D'Angelo G, and Raposo G (2018). Shedding light on the cell biology of extracellular vesicles. Nature Reviews Molecular Cell Biology 4, 213–228.
14. Andreu Z, and Yáñez-Mó M (2014). Tetraspanins in extracellular vesicle formation and function. Frontiers in Immunology 5, 442. [PubMed: 25278937]
15. Peden EM, and Barr MM (2005). The KLP-6 kinesin is required for male mating behaviors and polycystin localization in *Caenorhabditis elegans*. Current Biology 5, 394–404.
16. Morsci NS, and Barr MM (2011). Kinesin-3 KLP-6 regulates intraflagellar transport in male-specific cilia of *Caenorhabditis elegans*. Current Biology 14, 1239–1244.
17. Wang J, Schwartz HT, and Barr MM (2010). Functional specialization of sensory cilia by an RFX transcription factor isoform. Genetics 4, 1295–1307.
18. Wang J, Kaletsky R, Silva M, Williams A, Haas LA, Androwski RJ, Landis JN, Patrick C, Rashid A, Santiago-Martinez Det al. (2015). Cell-Specific Transcriptional Profiling of Ciliated Sensory Neurons Reveals Regulators of Behavior and Extracellular Vesicle Biogenesis. Current Biology 24, 3232–3238.
19. O'Hagan R, Silva M, Nguyen KCQ, Zhang W, Bellotti S, Ramadan YH, Hall DH, and Barr MM (2017). Glutamylation Regulates Transport, Specializes Function, and Sculpts the Structure of Cilia. Current Biology 22, 3430–3441.e6.
20. Akella JS, Silva M, Morsci NS, Nguyen KC, Rice WJ, Hall DH, and Barr MM (2019). Cell type-specific structural plasticity of the ciliary transition zone in *C. elegans*. Biology of the Cell 4, 95–107.
21. Chasnov JR, and Chow KL (2002). Why are there males in the hermaphroditic species *Caenorhabditis* elegans? Genetics 3, 983–994.
22. Simon JM, and Sternberg PW (2002). Evidence of a mate-finding cue in the hermaphrodite nematode *Caenorhabditis elegans*. PNAS 3, 1598–1603.
23. Lipton J, Kleemann G, Ghosh R, Lints R, and Emmons SW (2004). Mate Searching in *Caenorhabditis elegans*: A Genetic Model for Sex Drive in a Simple Invertebrate. J. Neurosci. 34, 7427–7434.
24. Barr MM, García LR, and Portman DS (2018). Sexual Dimorphism and Sex Differences in *Caenorhabditis elegans* Neuronal Development and Behavior. Genetics 3, 909–935.
25. Wang J, Nikonorova IA, Gu A, Sternberg PW, and Barr MM (2020). Release and targeting of polycystin-2-carrying ciliary extracellular vesicles. Current Biology 13, R755–R756.

26. Desai PB, Stuck MW, Lv B, and Pazour GJ (2020). Ubiquitin links smoothened to intraflagellar transport to regulate Hedgehog signaling. J. Cell Biol. 7, e201912104.
27. Hogan MC, Manganelli L, Woollard JR, Masyuk AI, Masyuk TV, Tammachote R, Huang BQ, Leontovich AA, Beito TG, Madden BJet al. (2009). Characterization of PKD protein-positive exosome-like vesicles. Journal of the American Society of Nephrology 2, 278–288.
28. Hogan MC, Bakeberg JL, Gainullin VG, Irazabal MV, Harmon AJ, Lieske JC, Charlesworth MC, Johnson KL, Madden BJ, Zenka RMet al. (2015). Identification of biomarkers for PKD1 using urinary exosomes. Journal of the American Society of Nephrology 7, 1661–1670.
29. Ma M, Tian X, Igarashi P, Pazour GJ, and Somlo S (2013). Loss of cilia suppresses cyst growth in genetic models of autosomal dominant polycystic kidney disease. Nat. Genet. 9, 1004–1012.
30. Wang J, and Barr MM (2018). Cell–cell communication via ciliary extracellular vesicles: clues from model systems. Essays Biochem. 2, 205–213.
31. Blacque OE, and Sanders AA (2014). Compartments within a compartment: What *C. elegans* can tell us about ciliary subdomain composition, biogenesis, function, and disease. Organogenesis 1, 126–137.
32. Carter SP, and Blacque OE (2019). Membrane retrieval, recycling and release pathways that organise and sculpt the ciliary membrane. Curr. Opin. Cell Biol. 133–139. [PubMed: 31146146]
33. Long H, Zhang F, Xu N, Liu G, Diener DR, Rosenbaum JL, and Huang K (2016). Comparative Analysis of Ciliary Membranes and Ectosomes. Current Biology 24, 3327–3335.
34. Diener DR, Lupetti P, and Rosenbaum JL (2015). Proteomic analysis of isolated ciliary transition zones reveals the presence of ESCRT proteins. Current Biology 3, 379–384.
35. Akella JS, Carter SP, Nguyen K, Tsiropoulou S, Moran AL, Silva M, Rizvi F, Kennedy BN, Hall DH, Barr MMet al. (2020). Ciliary RAB28 and the BBSome negatively regulate extracellular vesicle shedding. eLife 9, e50580. [PubMed: 32101165]
36. Raiders S, Black EC, Bae A, MacFarlane S, Klein M, Shaham S, and Singhvi A (2021). Glia actively sculpt sensory neurons by controlled phagocytosis to tune animal behavior. eLife 10, e63532. [PubMed: 33759761]
37. Wang J, and Barr MM (2016). Ciliary Extracellular Vesicles: Txt Msg Organelles. Cell. Mol. Neurobiol. 3, 449–457.
38. Perkins LA, Hedgecock EM, Thomson JN, and Culotti JG (1986). Mutant sensory cilia in the nematode *Caenorhabditis elegans*. Dev. Biol. 2, 456–487.
39. Sulston JE, Albertson DG, and Thomson JN (1980). The *Caenorhabditis elegans* male: Postembryonic development of nongonadal structures. Dev. Biol. 2, 542–576.
40. Ward S, Thomson N, White JG, and Brenner S (1975). Electron microscopical reconstruction of the anterior sensory anatomy of the nematode *Caenorhabditis elegans*. J. Comp. Neurol. 3, 313–337.
41. Bae YK, Kim E, L'Hernault SW, and Barr MM (2009). The CIL-1 PI 5-Phosphatase Localizes TRP Polycystins to Cilia and Activates Sperm in *C. elegans*. Current Biology 19, 1599–1607. [PubMed: 19781942]
42. Akella JS, and Barr MM (2020). The tubulin code specializes neuronal cilia for extracellular vesicle release. Developmental Neurobiology 81, 231–252. [PubMed: 33068333]
43. Scheidel N, Kennedy J, and Blacque OE (2018). Endosome maturation factors Rabenosyn5/VPS45 and caveolin-1 regulate ciliary membrane and polycystin-2 homeostasis. EMBO J. 37, e98248. [PubMed: 29572244]
44. Schou KB, Mogensen JB, Morthorst SK, Nielsen BS, Aleliunaite A, Serra-Marques A, Fürstenberg N, Saunier S, Bizet AA, Veland IRet al. (2017). KIF13B establishes a CAV1-enriched microdomain at the ciliary transition zone to promote Sonic hedgehog signalling. Nature Communications 8, 14177.
45. Morthorst SK, Christensen ST, and Pedersen LB (2018). Regulation of ciliary membrane protein trafficking and signaling by kinesin motor proteins. FEBS Journal 24, 4535–4564.
46. Zhukovsky MA, Filograna A, Luini A, Corda D, and Valente C (2019). Protein Amphipathic Helix Insertion: A Mechanism to Induce Membrane Fission. Frontiers in Cell and Developmental Biology 7, 291. [PubMed: 31921835]

47. Wickstead B, Gull K, and Richards TA (2010). Patterns of kinesin evolution reveal a complex ancestral eukaryote with a multifunctional cytoskeleton. BMC Evolutionary Biology 1, 110.

48. Moreno Y, Geary TG, and Tritten L (2021). When Secretomes Meet Anthelmintics: Lessons for Therapeutic Interventions. Trends Parasitol. 6, 468–475.

49. Loghry HJ, Yuan W, Zamanian M, Wheeler NJ, Day TA, and Kimber MJ (2020). Ivermectin inhibits extracellular vesicle secretion from parasitic nematodes. Journal of Extracellular Vesicles 2, e12036.

50. Dent JA, Smith MM, Vassilatis DK, and Avery L (2000). The genetics of ivermectin resistance in *Caenorhabditis elegans*. Proc. Natl. Acad. Sci. U. S. A. 6, 2674–2679.

51. Jauregui AR, Nguyen KCQ, Hall DH, and Barr MM (2008). The *Caenorhabditis elegans* nephrocystins act as global modifiers of cilium structure. J. Cell Biol. 5, 973–988.

52. Bae YK, Qin H, Knobel KM, Hu J, Rosenbaum JL, and Barr MM (2006). General and cell-type specific mechanisms target TRPP2/PKD-2 to cilia. Development 19, 3859–3870.

53. Brenner S (1974). The genetics of *Caenorhabditis elegans*. Genetics 1, 71–94.

54. Barr MM, DeModena J, Braun D, Nguyen CQ, Hall DH, and Sternberg PW (2001). The *Caenorhabditis elegans* autosomal dominant polycystic kidney disease gene homologs *lov-1* and *pkd-2* act in the same pathway. Current Biology 17, 1341–1346.

55. Dokshin GA, Ghanta KS, Piscopo KM, and Mello CC (2018). Robust Genome Editing with Short Single-Stranded and Long, Partially Single-Stranded DNA Donors in *Caenorhabditis elegans*. Genetics 3, 781–787.

56. Paix A, Folkmann A, Goldman DH, Kulaga H, Grzelak MJ, Rasoloson D, Paidemarry S, Green R, Reed RR, and Seydoux G (2017). Precision genome editing using synthesis-dependent repair of Cas9-induced DNA breaks. Proc. Natl. Acad. Sci. U. S. A. 50, e10745–e10754.

57. Haeussler M, Schönig K, Eckert H, Eschstruth A, Mianné J, Renaud J, Schneider-Maunoury S, Shkumatava A, Teboul L, Kent Jet al. (2016). Evaluation of off-target and on-target scoring algorithms and integration into the guide RNA selection tool CRISPOR. Genome Biol. 1, 148.

Highlights

- Cilia shed EVs at two sites: the base and tip
- Ciliary tip EV biogenesis requires cargo-enrichment, IFT kinesin-2, and kinesin-3
- Cilia shed heterogeneous EVs for signaling and biogenesis purposes
- *C. elegans* males dynamically modify content of environmentally released EVs

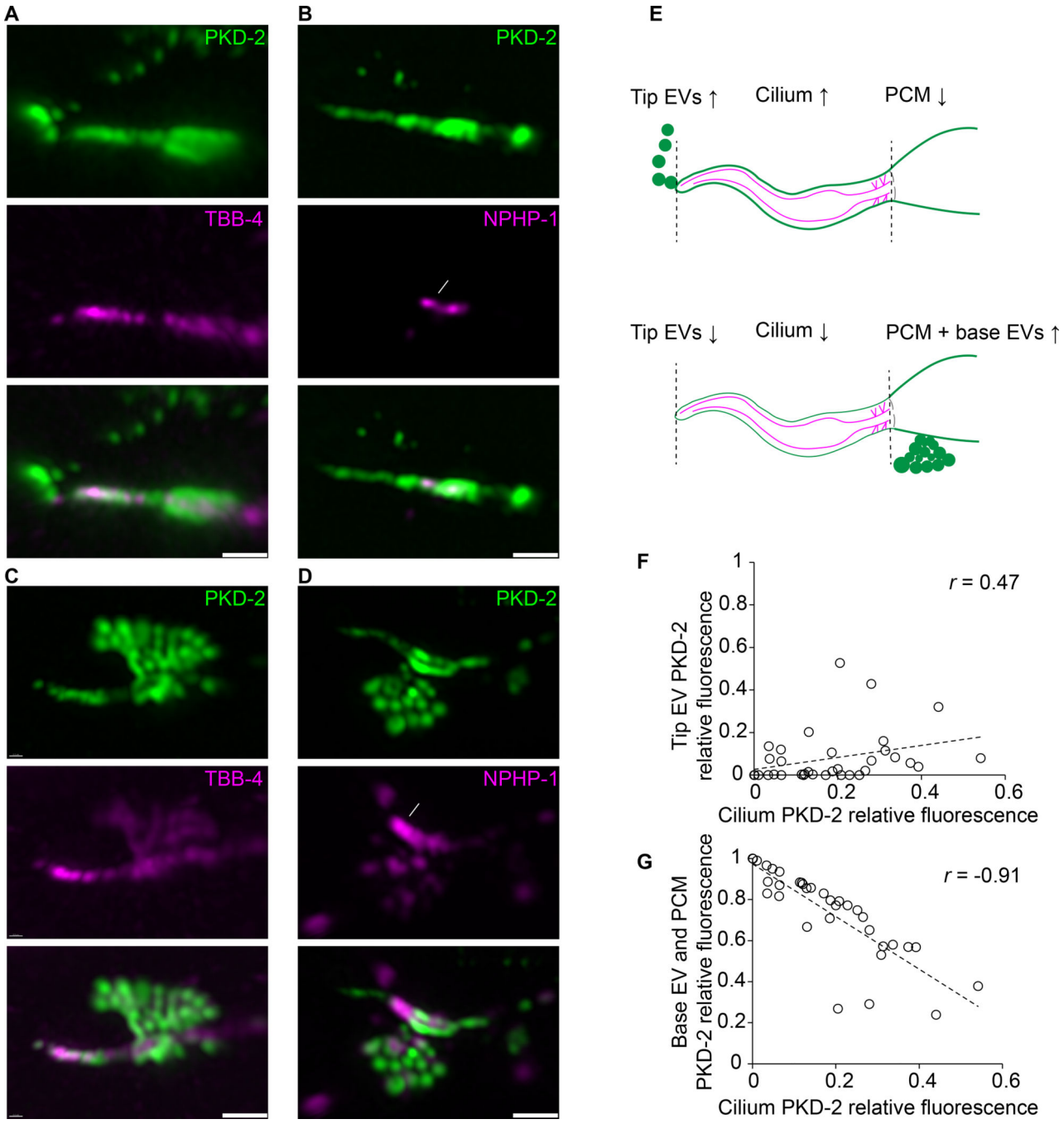

Figure 1: PKD-2 EVs are shed at two sites: the ciliary tip and base of the cephalic male CEM cilium.

A-D PKD-2:GFP EVs captured at the moment of shedding from the tip (in **A** and **B)** or from the base (in **C** and **D**) of the CEM cilium. The axoneme is labeled with β-tubulin TBB-4::tdTomato, transition zone is labeled with NPHP-1::dsRed. White arrowheads indicate environmental EVs outside the animal, white arrows point to the transition zone. Dashed white lines outline base EVs in the process of shedding, solid white lines indicate PCM, periciliary membrane this is situated below the transition zone.

E, Schematic cartoon showing the relationship between PKD-2 levels in ciliary tip EVs, the ciliary membrane and the region containing the PCM and ciliary base EVs.
F-G, Correlation plots showing that fluorescence intensity of the tip PKD-2::GFP EVs positively correlates with that of the ciliary shaft (**F**), whereas fluorescence intensity of the base PKD-2::GFP EVs inversely correlates with the presence of PKD-2::GFP at the ciliary shaft (**G**). Spearman test, 35 data pairs. $r = 0.47$, $p = 0.004$ for (**f**), $r = -0.91$, $p < 0.0001$ for (**G**). Each circle indicates relative fluorescence intensity of the compartment, i. e. the environmental EVs, the ciliary shaft or the ciliary base for each cilium.
Scale bars are 1 μm.
See also Table S1, Video S1–2.

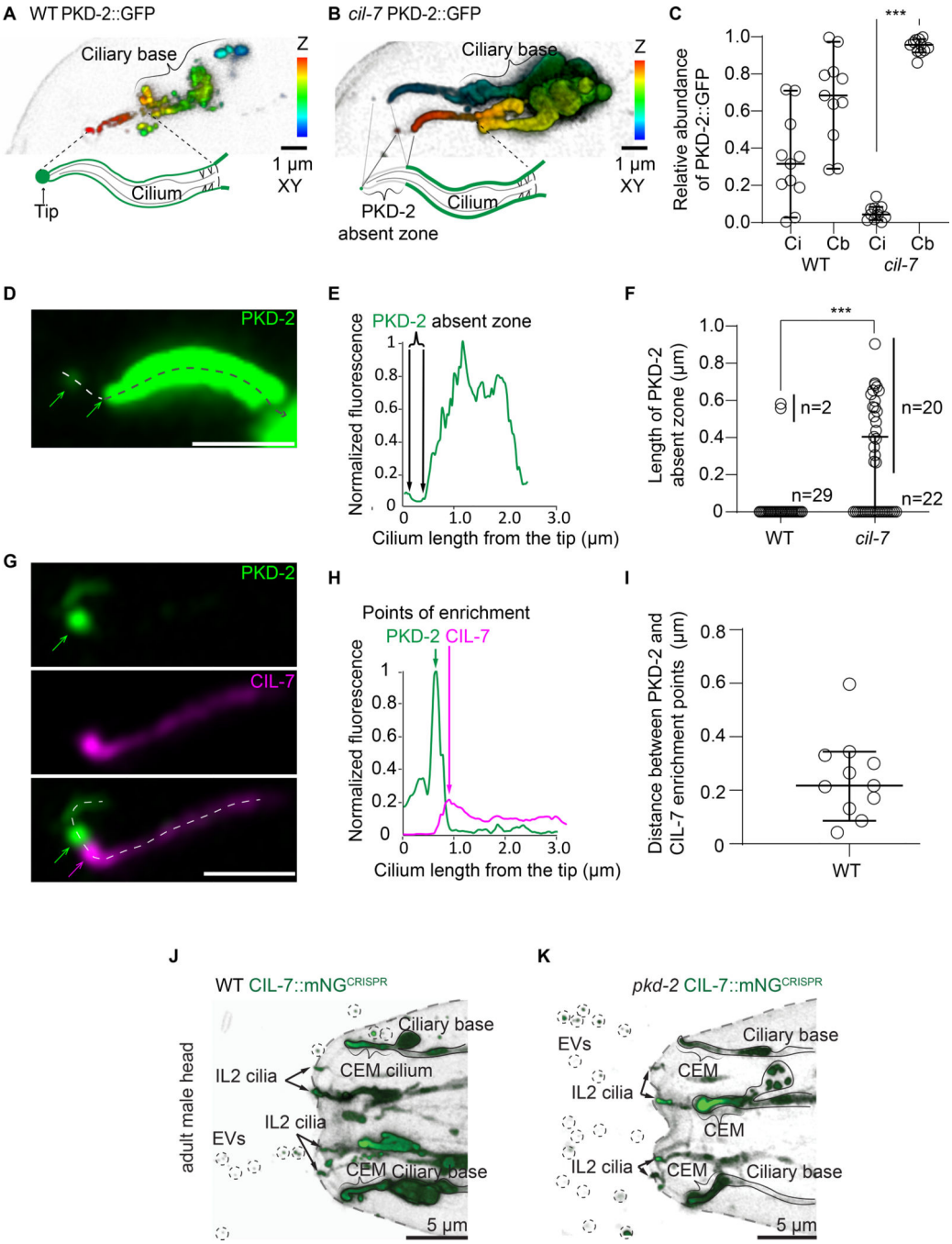

Figure 2. PKD-2 release from the tip of CEM cilium requires its distal ciliary enrichment mediated by CIL-7,but CIL-7 EV biogenesis is independent of PKD-2.

A-B, Depth coded 3D projections of PKD-2::GFP distribution in the CEM cilia in wild type (strain name PT621) and the *cil-7* mutant (strain name PT2681). In the wild type, PKD-2 is distributed evenly along the cilium including ciliary base, shaft, and tip. The *cil-7* mutant cilium lacks PKD-2::GFP at the tip and at the distal region, whereas considerable accumulations of PKD-2::GFP are observed at the ciliary shaft and the ciliary base.

C, Measured PKD-2::GFP relative fluorescence intensity distribution along ciliary shaft (Ci) and ciliary base of wild type and the *cil-7* mutant cilia. Each circle indicates the relative fluorescent intensity of the compartment for the cilium. The *cil-7* mutant demonstrates heavily skewed distribution of PKD-2 with significant accumulations at the ciliary base. ***$p<0.001$ by Kruskal-Wallis test with Dunn's multiple comparison, n=11 wild type and 11 *cil-7* mutant cilia.

D-E, Close-up image of PKD-2::GFP distribution along the *cil-7* mutant cilium. Dashed line with arrowhead indicates direction of fluorescent intensity profiling depicted in **E.**

F, The PKD-2 absent zone in the *cil-7* mutant reaches up to 1 μm, which is significantly larger than in most wild-type cilia. ***$p<0.001$ by Mann-Whitney test, n=31 wild type and 42 *cil-7* mutant cilia.

G, Representative image of the wild-type CEM cilium showing PKD-2::GFP enrichment at the ciliary tip. Newly formed string of tip EVs is labeled as EVs and indicated by white line; it extends from the PKD-2 enriched ciliary tip to above focal planes. Green and magenta arrows point to the corresponding positions of PKD-2 and CIL-7 enrichment points shown in **H**.

H, Fluorescent intensity profiling of the cilium from panel **G** shows that PKD-2 and CIL-7 are enriched at distinct locations positioned at 256 nm apart from each other.

I, Distances measured between PKD-2 and CIL-7 enrichment points at the distal parts of wild-type cilia, n=11.

All the plots show median values with 95% confidence intervals.

J-K, Representative images of *C. elegans* adult male head releasing CIL-7::mNeonGreen EVs in wild type and the *pkd-2* mutant. CIL-7::mNeonGreen transgenic animals were generated by CRISPR (Strain name for WT is PT3602, for *pkd-2* mutant is PT3621). In the wild type (**J**) and the *pkd-2* mutant (**K**) CIL-7 EVs are released by male-specific CEM cilia (outlined and indicated by figure bracket) and the sex shared IL2 cilia (arrows) in the head. Ciliary localization and EV biogenesis look similar in wild-type and *pkd-2* mutant males (n=5 animals for wild type, n=9 animals for the *pkd-2* mutant). Circles indicate environmentally released EVs. Scale bar, 5 μm.

See also Figure S1–4, Video S3.

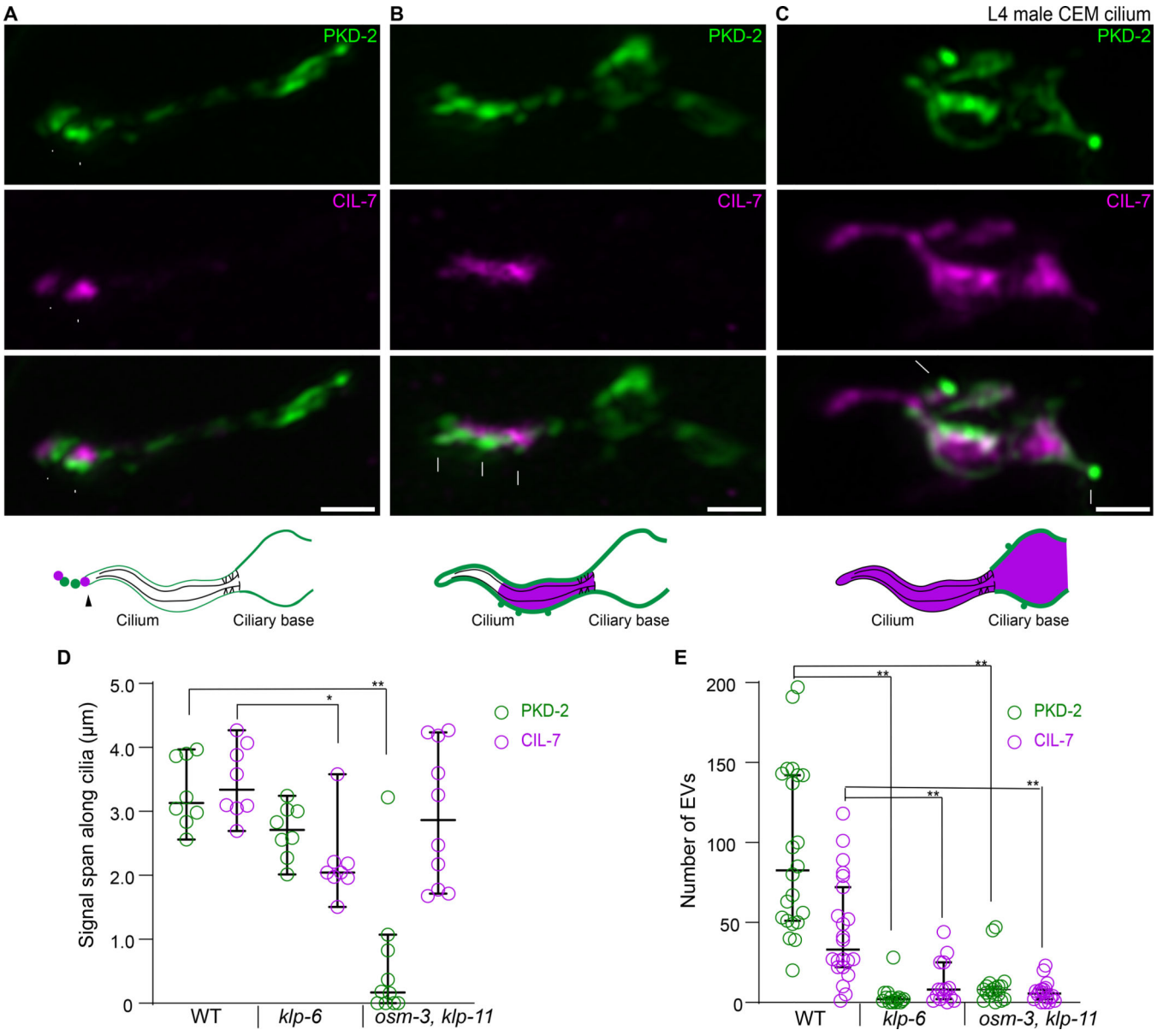

Figure 3. PKD-2 and CIL-7 require kinesin motors for ciliary tip localization.

A-C, Representative images of L4 male CEM cilia of wild type (**A**), kinesin-3 *klp-6* mutant (**B**), and kinesin-2 *osm-3 klp-11* double mutant (**C**). Top to bottom: PKD-2, CIL-7, merged channel, and cartoon summarizing the observed PKD-2 and CIL-7 localization.

A, In the wild type, PKD-2::GFP puncta are observed at the ciliary membrane and are enriched at the ciliary tip. The CIL-7 is mostly enriched at the ciliary tip at places of active EV biogenesis.

B, In the kinesin-3 *klp-6* mutant, PKD-2 and CIL-7 fail to reach the ciliary tip and are ectopically enriched at the ciliary shaft. Note that PKD-2::GFP is organized into small protrusions adjacent to CIL-7 enriched areas.

C, In the kinesin-2 *osm-3 klp-11* double mutant, PKD-2 fails to enter stunted cilia and accumulates considerably at the ciliary base. In contrast, CIL-7 locates to the cilium and

abnormally accumulates at the ciliary base. The CIL-7 enrichment at the base corresponds to the formation of PKD-2 enriched protrusions, similar to phenotype observed at the ciliary shaft of the *klp-6* mutant (**B**).

D, Quantification of the length of PKD-2 and CIL-7 along the cilia of wild type, *klp-6*, and *osm-3 klp-11* animals. CIL-7, but not PKD-2, traverses a significantly shorter distance in the *klp-6* mutant compared to wild type. PKD-2 localization is significantly affected in the *osm-3 klp-11* double mutant, but not in the *klp-6* mutant.

E, Quantification of number of EVs labeled by PKD-2 and CIL-7 in late L4 male tail molting cuticle. Each data point represents total EV numbers in one animal. *klp-6* and *osm-3 klp-11* mutants are defective in both PKD-2 and CIL-7 EV release.

Median values with 95% confidence intervals are indicated. *$p < 0.05$, ** $p<0.01$ by Kruskal-Wallis test with Dunn's multiple comparison, n=8, 8, and 10 for wild type, *klp-6,* and *osm-3 klp-11* in **D**, n=22, 15 and 18 for wild type, *klp-6* mutant, and *osm-3 klp-11* double mutant in **E**.

Scale bars are 1 μm.

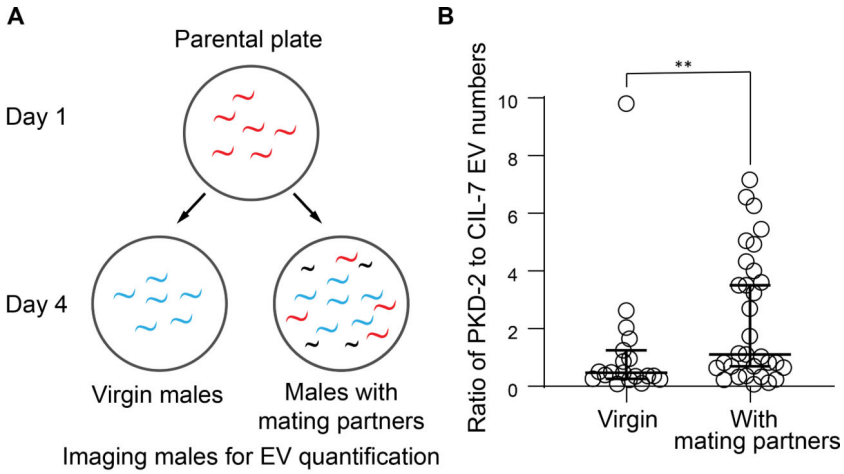

C

Male head PKD-2 and CIL-7 EVs quantification

EV marker	EV number (mean ± stdev)		n
	Virgin	With mating partners	
PKD-2	28.7 ± 31.4	47.9 ± 64.4	21
CIL-7	36.9 ± 33.9	26.6 ± 33.0	31

Figure 4. *C. elegans* males dynamically modify content of environmentally released EVs.

A, Scheme of experimental design for PKD-2 and CIL-7 EVs quantification in the presence or absence of mating partners. Males were isolated from a mixed population at the larval stage L4 and were imaged as adult virgin males alongside adult males picked from the mixed population with adult hermaphrodites.

B, The ratio of PKD-2 to CIL-7 EV numbers is significantly increased in males cultured in mixed population as compared to isolated virgin males. **P<0.01 by Mann Whitney test, n=19 for isolated and 31 for mixed population conditions.

C, Male head PKD-2 and CIL-7 EVs quantification in the presence or absence of mating partners. The increased ratio of PKD-2 to CIL-7 EVs is not simply due to an increase in the number of EVs released by the CEMs when males are exposed to hermaphrodite mating partners. Furthermore, the IL2 neurons produce a negligible amount of EVs that do not contribute substantially to the entire pool of CIL-7 EVs. This table shows that the number of CIL-7 EVs released by males exposed to mating partners decreased when compared to virgin males.

See also Figure S2, 4.

Key Resources Table

REAGENT or RESOURCE
Bacterial Strains
E. coli, OP50 strain
Chemicals, Peptides, and Recombinant Proteins
Levamisole
Agarose
Experimental Models: Organisms/Strains
Strain name
C. elegans Strain PT1435: *pha-1(e2123) III; myIs1 IV; him-5(e1490) V; myEx552 [Ppkd-2::*TBB-4*::tdTomato]*
C. elegans Strain PT823: *pha-1(e2123) III; myIs1* [PKD-2::GFP+P*unc-122*::GFP]*IV; him-5(e1490)V; myEx431 [Pnphp-1::*NPHP-1::dsRED]
C. elegans Strain PT621: *him-5(e1490) myIs4 [PKD-2::GFP+Punc-122::GFP]V*
C. elegans Strain PT3112: *pha-1(e2123) III; him-5(e1490) V myIs4V; myEx888[CIL-7::tagRFP + pBX1].*
C. elegans Strain PT3383: *klp-6(my8) III; him-5(e1490) myIs4V; myEx888[CIL-7::tagRFP + pBX1]*
C. elegans Strain PT3380: *pha-1(e2123) III; osm-3(p802) klp-11(tm324)IV; him-5(e1490) myIs4V; myEx888[CIL-7::tagRFP + pBX1]*
C. elegans Strain PT2681: *cil-7(tm5848) I; myIs1*[PKD-2::GFP+P*unc-122*::GFP] *IV; him-5(e1490)V*
C. elegans Strain PT3602: *cil-7(my61[cil-7::mNG])I; him-5(e1490) V*
C. elegans Strain PT3621: *cil-7(my61[cil-7::mNG])I; pkd-2(sy606)IV; him-5(e1490) V*
Software and Algorithms
Metamorph
Zen Blue 2.0
Zen Black 2.0
Imaris 9.5
Prism 8
Python 3
Code for calculating distance between centroids of EV particles and EV colocalization analysis
Oligonucleotides

REAGENT or RESOURCE
5’-ATGGATACGCTAACAACTTGGGCTGGGAGTCGATACATGGT-3’
5’-CAGCTCTTCGCCCTTAGACACATGATGTGCAGACTTCTTCTTTC-3’
5’ – CTCCATTGGAGCAACCTGTCAAATCTGGAAAGAAGAAGTCTGCACATCATGGAGGTGGCGGATCTGGAGGTGGAGGCTCTGGAGGAGGTGGATCTATGGTGTCGA – 3’
5’ – ATCACACAAAAATAGGCTGTTAAATGAAAATTATCGCAGTGGCATCTTATCGT AGCTACTTGTAGAGTTCATCCATTC – 3’
5’- TGACTACGATAAGATGCCAC – 3’
Recombinant DNA
Plasmid [CIL-7::tagRFP]